REPORT DOCUMENTATION PAGE

Form Approved
OMB No. 0704-0188

1. REPORT DATE (DD-MM-YYYY)	2. REPORT TYPE	3. DATES COVERED (From - To)
20-05-2004	REPRINT	

4. TITLE AND SUBTITLE
Reactions of O^+ with C_nH_{2n+2}, n=2-4: A Guided-Ion Beam Study

5a. CONTRACT NUMBER

5b. GRANT NUMBER

5c. PROGRAM ELEMENT NUMBER
61102F

6. AUTHOR(S)
D.J. Levandier*, Y. Chiu*, and R.A. Dressler

5d. PROJECT NUMBER
2303

5e. TASK NUMBER
RS

5f. WORK UNIT NUMBER
A1

7. PERFORMING ORGANIZATION NAME(S) AND ADDRESS(ES)
Air Force Research Laboratory/VSBXT
29 Randolph Road
Hanscom AFB MA 01731-3010

8. PERFORMING ORGANIZATION REPORT NUMBER
AFRL-VS-HA-TR-2004-1097

9. SPONSORING / MONITORING AGENCY NAME(S) AND ADDRESS(ES)

10. SPONSOR/MONITOR'S ACRONYM(S)
AFRL/VSBXT

11. SPONSOR/MONITOR'S REPORT NUMBER(S)

12. DISTRIBUTION / AVAILABILITY STATEMENT
Approved for Public Release; Distribution Unlimited

*Inst Sci Res, Boston College, Chestnut Hill, MA

13. SUPPLEMENTARY NOTES
REPRINTED FROM: JOURNAL OF CHEMICAL PHYSICS, Vol 120, No. 15, pp 6999-7007, 15 Apr 2004.

14. ABSTRACT

We have measured absolute reaction cross sections for the interaction of O^+ with ethane, propane, and *n*-butane at collision energies in the range from near thermal to approximately 20 eV, using the guided-ion beam (GIB) technique. We have also measured product recoil velocity distributions using the GIB time-of-flight (TOF) technique for several product ions at a series of collision energies. The total cross sections for each alkane are in excess of 100 $Å^2$ at energies below ~2 eV, and in each case several ionic products arise. The large cross sections suggest reactions that are dominated by large impact parameter collisions, as is consistent with a scenario in which the many products derive from a near-resonant, dissociative charge-transfer process that leads to several fragmentation pathways. The recoil velocities, which indicate product ions with largely thermal velocity distributions, support this picture. Several product ions, most notably the $C_2H_3^+$ fragment for each of the alkanes, exhibit enhanced reaction efficiency as collision energy increases, which can be largely attributed to endothermic channels within the dissociative charge-transfer mechanism.

15. SUBJECT TERMS
Ion-molecule reactions; Alkanes; Ionospheric ions; Materials degradation; Guided-ion beams; Charge transfer; Dissociative charge transfer; Recoil velocities

16. SECURITY CLASSIFICATION OF:			17. LIMITATION OF ABSTRACT	18. NUMBER OF PAGES	19a. NAME OF RESPONSIBLE PERSON
a. REPORT	b. ABSTRACT	c. THIS PAGE			R. Dressler
UNCLAS	UNCLAS	UNCLAS	SAR	9	19b. TELEPHONE NUMBER (include area code) 781-377-2332

JOURNAL OF CHEMICAL PHYSICS VOLUME 120, NUMBER 15 15 APRIL 2004

Reactions of O^+ with C_nH_{2n+2}, $n=2-4$: A guided-ion beam study

Dale J. Levandier,[a),b)] Yu-hui Chiu,[a)] and Rainer A. Dressler
Space Vehicles Directorate, Air Force Research Laboratory, Hanscom AFB, Massachusetts 01731

(Received 2 October 2003; accepted 15 January 2004)

We have measured absolute reaction cross sections for the interaction of O^+ with ethane, propane, and *n*-butane at collision energies in the range from near thermal to approximately 20 eV, using the guided-ion beam (GIB) technique. We have also measured product recoil velocity distributions using the GIB time-of-flight (TOF) technique for several product ions at a series of collision energies. The total cross sections for each alkane are in excess of 100 $Å^2$ at energies below ~2 eV, and in each case several ionic products arise. The large cross sections suggest reactions that are dominated by large impact parameter collisions, as is consistent with a scenario in which the many products derive from a near-resonant, dissociative charge-transfer process that leads to several fragmentation pathways. The recoil velocities, which indicate product ions with largely thermal velocity distributions, support this picture. Several product ions, most notably the $C_2H_3^+$ fragment for each of the alkanes, exhibit enhanced reaction efficiency as collision energy increases, which can be largely attributed to endothermic channels within the dissociative charge-transfer mechanism.
 [DOI: 10.1063/1.1667459]

INTRODUCTION

Our interest in the reactions of ethane, propane, and *n*-butane with O^+ derives largely from the effort to understand the effects of exposure of spacecraft to the low-Earth orbit (LEO) environment, in which this ion is the most abundant. In particular, these gas-phase reactions are intended to provide a basis for understanding the origin of polymer erosion at LEO conditions. An overview of the phenomena observed in ion–organic surface interactions was given by Cooks *et al.*[1] Other areas of interest are hydrocarbon combustion, where reactions of air plasma ions with alkanes may be important,[2,3] and reactions in planetary atmospheres.[4]

Exothermic charge-transfer reactions of small alkanes have been the subject of a number of studies,[5–9] in part to investigate the characteristics of the exothermic charge-transfer process itself, as well as to shed light on the fragmentation channels observed when the alkanes are ionized.[10–14] Further, reactions of alkanes with ions in which charge transfer is endothermic have also been studied extensively.[2,9,15,16]

Charge transfer is exothermic for the three $O^+(^4S)$ reaction systems of the present study:[17]

$$O^+(^4S_{3/2})+C_2H_6(\tilde{X})\rightarrow O(^3P_2)+C_2H_6^+(\tilde{X}), \quad \Delta E=-2.09 \text{ eV}, \tag{1}$$

$$O^+(^4S_{3/2})+C_3H_8(\tilde{X})\rightarrow O(^3P_2)+C_3H_8^+(\tilde{X}), \quad \Delta E=-2.67 \text{ eV}, \tag{2}$$

$$O^+(^4S_{3/2})+n\text{-}C_4H_{10}(\tilde{X})\rightarrow O(^3P_2)+n\text{-}C_4H_{10}^+(\tilde{X}), \quad \Delta E=-3.09 \text{ eV}. \tag{3}$$

These collision systems therefore may be expected to be dominated by charge-transfer effects, as has been observed in a selected ion flow tube–drift study by Praxmarer *et al.*,[6] in which reactions of these same alkanes with a range of ions were examined. It is interesting to note, however, that a large number of reaction channels that may be characterized as involving formation of OH (abstraction) or of C–O bonds (insertion) are more exothermic,[17] however, these channels have so far not been observed.[18]

In this paper, we present the detailed results of a guided-ion beam (GIB) study of $O^+(^4S_{3/2})$ reactions with ethane, propane, and *n*-butane, in which we have measured absolute reaction cross sections at near-thermal to hyperthermal collision energies and recoil velocity distributions of product ions at selected collision energies. The latter are particularly important for distinguishing whether the products are associated with a chemical reaction or merely a dissociative charge-transfer process.

EXPERIMENT

The instrument used in this study has been discussed in detail previously,[19] so only a brief description is given here. An rf octopole ion guide is located between the two mass filters in a tandem mass spectrometer. The ion guide has two stages, the first octopole of length 7.4 cm and the second of length 16.7 cm, and passes through a 3.5-cm-long collision cell located so that its exit is at the junction of the two octopole stages. Ions are conveyed from the first mass filter to the first octopole stage, and from the second octopole stage to the second mass filter by injection and extraction lens systems, respectively.

[a)]Also at Institute for Scientific Research, Boston College, Chestnut Hill, MA 02159.
[b)]Author to whom correspondence should be addressed.

Electron impact on CO_2 is used to generate O^+ ions via dissociative ionization. The primary ion beam is produced in almost exclusively[20,21] ($\geq$99%) the ground state $O^+(^4S)$ by keeping the electron energy at ~20 eV, which is 2.3 eV below the appearance potential for $O^+(^2D)$. Primary ions are mass selected in the first mass spectrometer and are then injected into the first octopole at the desired kinetic energy. Unreacted primary ions and ions produced in reactions with the target gas in the collision cell pass into the second octopole, which is typically biased 0.4–0.5 V below the first octopole to aid in the extraction of thermal product ions from the cell. At the exit of the second octopole, primary and secondary ions are injected into a quadrupole mass filter for mass analysis. Secondary reactions in the collision cell, owing to the large cross sections for reactions of smaller hydrocarbon ions (fragments, here) with alkanes,[22] are minimized by maintaining target gas pressures in the range of 0.08–0.10 mTorr, and by periodically turning off the rf potential to allow trapped low-energy ions to escape the octopole volume.[21] It must also be noted that the acceleration of thermal ions into the second octopole operated at a lower bias potential than the first also significantly reduces secondary reactions with background gas. The ion-beam energy is known to better than ±0.1 eV, with beam spreads typically of ~0.25 eV full width at half maximum, as measured by the retarding potential method and by time of flight.

As described previously,[19] absolute cross sections are determined by integrating the mass spectrometer signal intensities for the product and transmitted primary ions, monitoring the pressure of the target gas, and using the low-density limit of the Lambert–Beer expression. Due to discrimination of higher masses at high mass resolution in the second mass filter, the cross sections for individual product masses were measured at high mass resolution (baseline separation of product masses), to obtain product branching ratios, then these results were scaled to cross sections measured at sufficiently low mass resolution to eliminate the discrimination. Errors in the absolute cross sections, based in part on periodic calibration of the apparatus using the accepted standard reaction, $Ar^+ + D_2 \rightarrow ArD^+ + D$,[19,23] are estimated to be of the order of ±30%.

Product ion time-of-flight (TOF) spectra are measured by pulsing the primary ion beam, using a 3–5 μs ion beam pulse width, and measuring the flight time of product ions arriving at the detector. A ring-shaped electrode, surrounding the octopole at the entrance of the collision cell, is kept at ~100 V above the dc potential of the first octopole so that the small penetrating field (~0.1 V) reflects thermal product ions with "backwards" laboratory velocities. Very slow ions, which would otherwise result in a background signal in subsequent pulse cycles, are eliminated at the end of each cycle by briefly turning off the octopole rf potential.

Ethane (CP) was obtained from Scientific Gas Products, and propane and *n*-butane (UHP) from Matheson; the gases were used as delivered.

RESULTS

Figures 1–3 show the absolute cross sections for the ionic products of reactions of O^+ with C_2H_6, C_3H_8, and n-C_4H_{10}, respectively, at collision, or relative, energies (E_T) from near thermal to ~20 eV. In each case the total and Langevin–Gioumousis–Stevenson[24] (LGS) cross sections are shown, and in Fig. 1 the result derived from the thermal rate constant for $O^+ + C_2H_6$, determined in a flowing afterglow experiment at 298 K by Mackay *et al.*,[18] is also indicated. The total $O^+ + C_2H_6$ cross section agrees with the earlier work to within the combined limits of experimental error. The LGS cross sections are somewhat larger than the total cross sections at the lowest energies where capture dynamics apply. Figures 2(b) and 3(b) show the cross sections

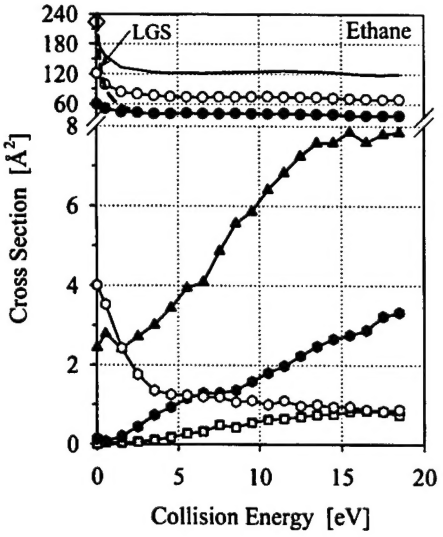

FIG. 1. Absolute cross sections for product ions derived from O^+ + ethane reactions as a function of collision, or relative, energy (E_T). The product ion masses (and their plot symbols) are 14 amu (▩), 26 amu (●), 27 amu (▲), 28 amu (○), 29 amu (●), and 30 amu (○). Note that these plot symbols are used to represent the same ion masses throughout this work. The solid curve is the total O^+ +ethane cross section, the heavy dashed curve is the calculated Langevin–Gioumousis–Stevenson (LGS) cross section, and the large diamond symbol represents the cross section derived from the thermal rate constant for O^+ + ethane (Ref. 18).

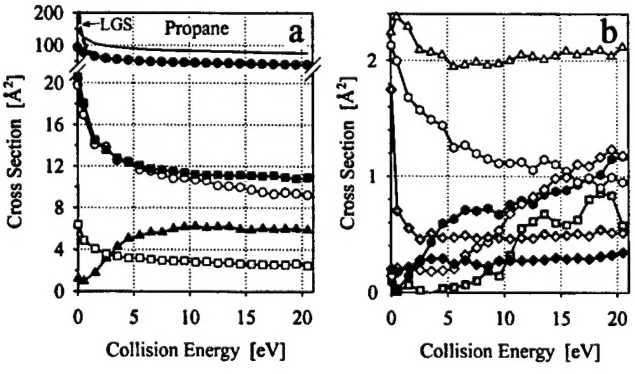

FIG. 2. Absolute cross sections for product ions derived from O^+ + propane reactions as a function of collision, or relative, energy (E_T). The product ion masses (and their plot symbols) are 14 amu (▩), 26 amu (●), 27 amu (▲), 28 amu (○), 29 amu (●), 30 amu (○), 39 amu (◇), 40 amu (◆), 41 amu (△), 42 amu (▩), 43 amu (■), and 44 amu (◆). Note that these plot symbols are used to represent the same ion masses throughout this work. Panel (a) contains the cross sections for the more efficient channels, as well as the total (solid line) and LGS cross sections (heavy dashed line). Panel (b) contains the cross sections for the minor channels.

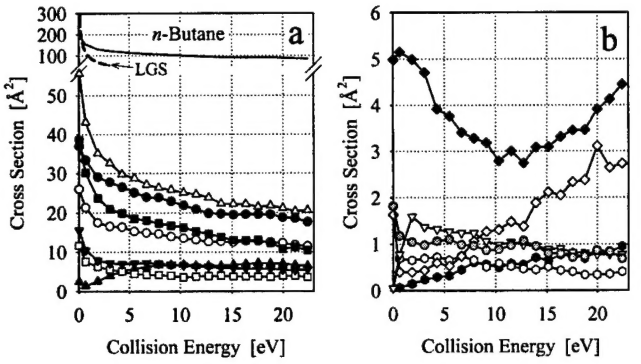

FIG. 3. Absolute cross sections for product ions derived from $O^+ + n$-butane reactions as a function of collision, or relative, energy (E_T). The product ion masses (and their plot symbols) are 26 amu (●), 27 amu (▲), 28 amu (○), 29 amu (●), 30 amu (○), 39 amu (◇), 40 amu (◆), 41 amu (△), 42 amu (▒), 43 amu (■), 56 amu (▽), 57 amu (▼), and 58 amu (▒). Note that these plot symbols are used to represent the same ion masses throughout this work. Panel (a) contains the cross sections for the more efficient channels, as well as the total (solid line) and LGS cross sections (heavy dashed line). Panel (b) contains the cross sections for the minor channels.

for the minor channels of the reactions with the two larger alkanes. None of the cross sections is corrected for the natural deuterium abundance.

For all systems the total cross sections become fairly independent of collision energy above 5 eV. At these energies, the magnitudes of the total cross sections are approximately 120, 80, and 90 Å^2, for ethane, propane, and *n*-butane, respectively. Table I indicates the product ion masses detected for each of the alkanes, as well as their branching fractions (expressed as a percentage) at 0.1 eV. Also shown in Table I are the chemical formula for each product ion mass and reaction energies, assuming that the reactions are dominated by a dissociative charge-transfer mechanism (see Discussion, below). In the remainder of this paper, indicated reaction energies for channels of interest are relative to the respective reagents in reactions 1, 2, and 3. In several instances, reaction energies in the text are denoted by "$\geqslant$" to indicate the lowest possible energy pathway, since a given product ion may arise by different mechanisms and may involve products with several possible isomers.

The cross-section data for the individual product ions from each of the alkanes merit closer inspection. In Fig. 1, for reaction with ethane, the largest cross sections correspond to $C_2H_4^+$ and $C_2H_5^+$, and have an energy dependence similar to the weaker channel associated with the charge-transfer product ion, $C_2H_6^+$. The cross sections for the $C_2H_3^+$, $C_2H_2^+$, and CH_2^+ products exhibit an enhancement with collision energy. In the case of $C_2H_3^+$, the present data indicate that this channel proceeds with measurable efficiency at the lowest collision energy studied, whereas the smaller channels do not, instead displaying a threshold behavior.

These two general trends are also observed for the reactions with propane and *n*-butane, respectively. In Fig. 2(a), the four largest product cross sections in reactions of propane at low energies lead to formation of $C_2H_5^+$, $C_3H_7^+$, $C_2H_4^+$, and $C_3H_6^+$, and have the same general energy dependence as

TABLE I. Branching fractions (%; upper line), for $E_T = 0.1$ eV, and reaction energies (eV; lower line), assuming the dissociative charge-transfer mechanism (see Discussion), for the observed product ions resulting from reactions of O^+ with C_2H_6, C_3H_8, and n-C_4H_{10}. The mass (amu) and formula are given for each product ion. The values in parentheses for the 28- and 29-amu products of ethane reactions are the branching fractions from previous work (Ref. 18).

Mass/formula	C_2H_6	C_3H_8	n-C_4H_{10}
14/CH_2^+	~0	~0	
	0.85	0.96	
26/$C_2H_2^+$	~0	~0	~0
	1.02	0.46	0.59
27/$C_2H_3^+$	1	1	1
	1.04	0.50	0.44
28/$C_2H_4^+$	65 (70)	13	13
	−1.70	−2.26	−2.13
29/$C_2H_5^+$	32 (30)	63	19
	−1.14	−1.67	−1.73
30/$C_2H_6^+$	2	<2	~0
	−2.09	2.16	−1.11
39/$C_3H_3^+$		~0	1
		0.87	0.35
40/$C_3H_4^+$		~0	<3
		−0.86	−1.41
41/$C_3H_5^+$		<2	28
		−0.47	−0.99
42/$C_3H_6^+$		4	6
		−2.60	−3.14
43/$C_3H_7^+$		14	20
		−2.00	−1.66
44/$C_3H_8^+$		1	
		−2.67	
56/$C_4H_8^+$			~0
			−3.33
57/$C_4H_9^+$			8
			−2.86
58/$C_4H_{10}^+$			1
			−3.09

the charge-transfer product cross section in Fig. 2(b). In contrast, the cross sections for $C_2H_3^+$ in Fig. 2(a) and $C_2H_2^+$, $C_3H_3^+$, $C_3H_4^+$, and CH_2^+ in Fig. 2(b) show enhancement with increasing collision energy. As in the ethane experiment, the $C_2H_3^+$ cross section indicates non-negligible efficiency at low energy, and increases to a relatively large value at the highest collision energies.

For butane [Fig. 3(a)] the largest product cross sections at low energy are $C_3H_5^+$, $C_3H_7^+$, $C_2H_5^+$, $C_2H_4^+$, $C_4H_9^+$, and $C_3H_6^+$. The energy dependences of these products are similar to that of the $C_4H_{10}^+$ charge-transfer product. The $C_2H_3^+$ cross section in Fig. 3(a) exhibits the same behavior as is seen for the smaller alkanes. For production of $C_3H_3^+$, in Fig. 3(b), the cross section shows a similar enhancement with collision energy, while the other minor products, $C_2H_2^+$, $C_2H_6^+$, $C_3H_4^+$, and $C_4H_8^+$, have cross sections that do not clearly follow either of the trends described above.

The present results do not show evidence for oxygen insertion products. To help confirm the assignment of the product ion masses to hydrocarbon species, with no oxygen insertion, we conducted a study with perdeuteropropane, C_3D_8. Mass spectra of secondary ions were recorded at $O^+ + C_3D_8$ collision energies of 0.4 and 11.7 eV, the results

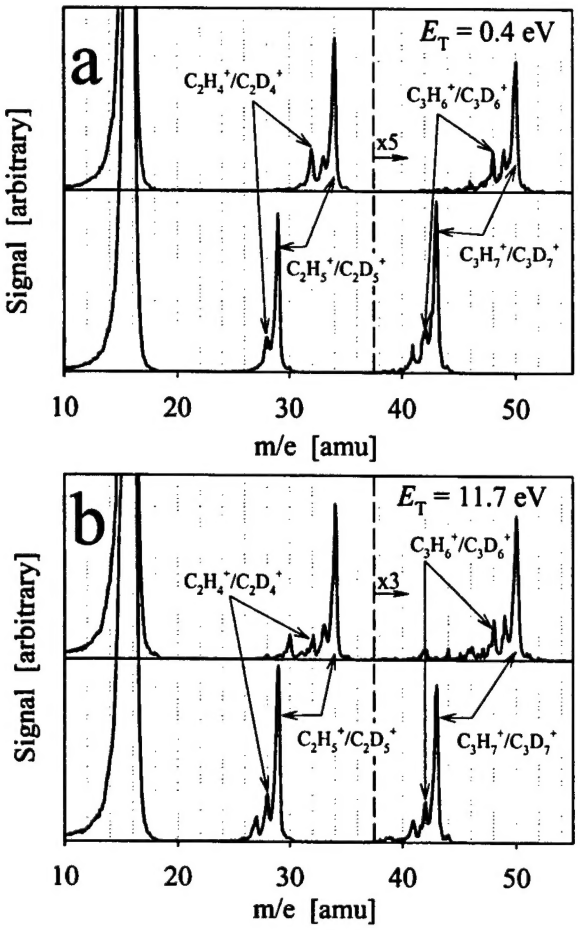

FIG. 4. Comparison of mass spectra for reactions of O^+ with C_3H_8 and C_3D_8 at (a) 0.4-eV and (b) 11.7-eV collision energies. The sets of arrows indicate corresponding pairs of normal and perdeutero products, confirming the assignment of hydrocarbon formulas to the observed product masses. The vertical dashed lines, in (a) and (b), delineate the indicated expansion of signal scale at higher mass.

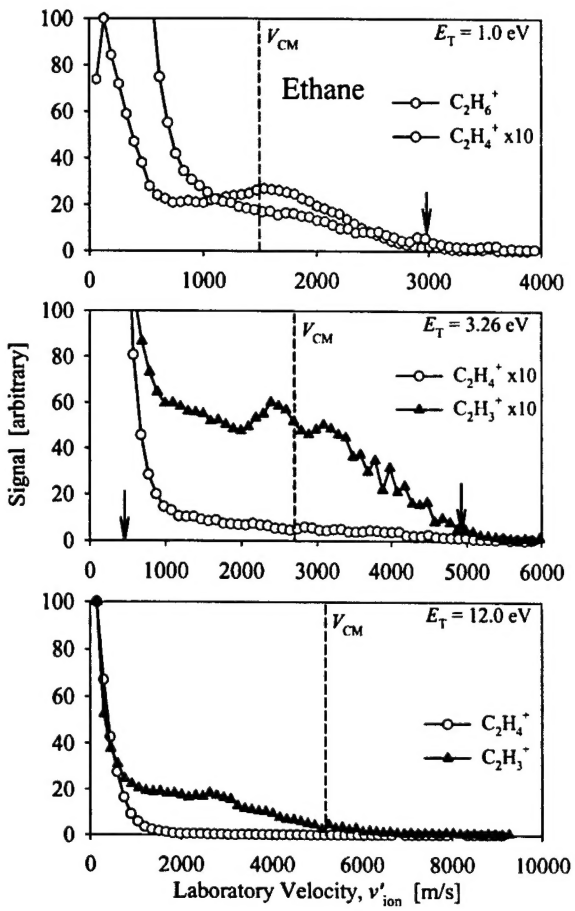

FIG. 5. Time-of-flight data for the indicated product ions derived from reaction of O^+ + ethane, at collision energies of 1.0, 3.26, and 12.0 eV. The data have been transformed to the laboratory velocity frame. The dashed vertical line, in each plot, indicates the velocity of the center of mass of the collision system. In the top plot, the arrow indicates the maximum possible laboratory velocity for elastically scattered $C_2H_6^+$. In the middle plot, the arrows indicate the maximum forward and backward velocities, with respect to V_{CM}, for $C_2H_3^+$, assuming that 1.04 eV of the collisions energy is converted to internal energy and that dissociation occurs with zero recoil energy.

of which are shown in Figs. 4(a) and 4(b), respectively. To obtain better signal levels at the higher masses, these data were obtained at somewhat lower mass resolution than was used for the other results presented here. The $C_2H_4^+$ product may be taken as an illustrative example. The masses of this ion and of CO^+ [$\Delta E \geq -3.8$ eV (Ref. 17)] are the same, however, in the reaction with the perdeuteropropane, the corresponding product is clearly shifted to the $C_2D_4^+$ mass, with negligible signal at the $m/z=28$ location. Similarly, $C_2H_5^+$ and HCO^+ [$\Delta E \geq -5.8$ eV (Ref. 17)] have the same masses, but the perdeuteropropane reaction indicates production of the corresponding deuterated ethyl ion. Similar arguments support the assignment of the larger products. The mass spectral data also indicate $\sim 10\%$ C_3HD_7/C_3D_8 impurity, which does not interfere with the current analysis.

Figures 5–7 show the TOF results for selected products of reactions with ethane, propane, and *n*-butane, respectively. The data, transformed from the TOF measurements, are displayed as product ion laboratory velocity distributions for velocity components parallel to the incident ion beam, v'_{ion}. The velocity distributions are of arbitrary scale, normalized so that the maximum amplitude is set at 100. For each target gas, spectra were obtained at low, medium, and higher collision energies, where the medium energy was chosen to correspond to a relative velocity of 7.8 km/s, typical of low-Earth orbit interactions. In each spectrum, the vertical dashed line represents the velocity of the center of mass of the colliding system, V_{CM}, which constitutes the origin of the center-of-mass reference frame. That is, taking the direction of the primary ion beam as forward in the center-of-mass frame, product ions with laboratory velocities in excess of V_{CM} exhibit recoil velocities in the forward hemisphere, while slower ions are backscattered.

In Fig. 5, for ethane reactions at 1.0 eV, TOF results are shown for two of the ions whose cross sections decline with collision energy at low energies, $C_2H_6^+$ and $C_2H_4^+$. The $C_2H_6^+$ velocity distribution is clearly bimodal, with a low-velocity component and a substantial contribution from faster ions that is peaked near V_{CM}. The arrow in this plot corresponds to the maximum laboratory velocity of elastically scattered $C_2H_6^+$. The dip at low laboratory velocity may be due to secondary reactions which, due to residence time, would most affect the lowest velocities.

The $C_2H_4^+$ TOF data for ethane reaction at 1.0 eV are

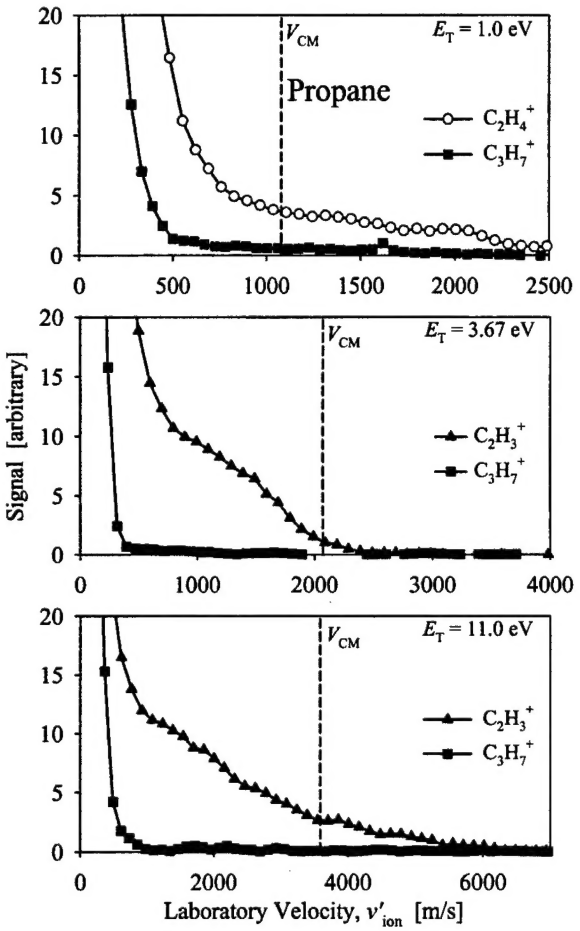

FIG. 6. Time-of-flight data for the indicated product ions derived from reaction of O^+ + propane, at collision energies of 1.0, 3.67, and 11.0 eV. The data have been transformed to the laboratory velocity frame. The dashed vertical line, in each plot, indicates the velocity of the center of mass of the collision system. Note that the velocity spectra are normalized so that their maxima equal 100.

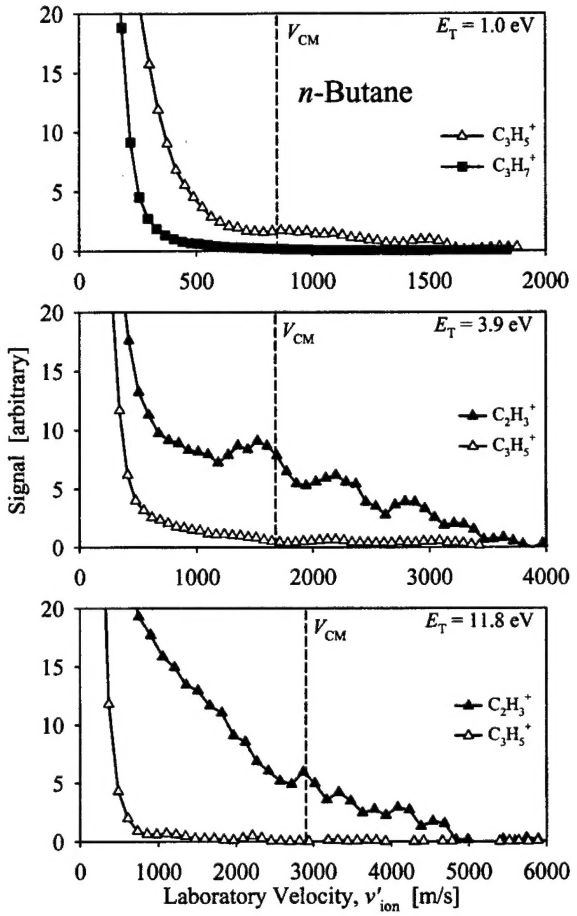

FIG. 7. Time-of-flight data for the indicated product ions derived from reaction of $O^+ + n$-butane, at collision energies of 1.0, 3.9, and 11.8 eV. The data have been transformed to the laboratory velocity frame. The dashed vertical line, in each plot, indicates the velocity of the center of mass of the collision system. Note that the velocity spectra are normalized so that their maxima equal 100.

dominated by the thermal component, with only a small faster contribution that tails to the forward direction. At the higher collision energies studied, the fast component for this product diminishes with respect to the dominant thermal portion, as would be expected if the former involved complex-mediated collisions. TOF data for the $C_2H_3^+$ product were obtained at the higher collision energies and, along with a large thermal contribution, show a persistent fast component even at 12.0 eV collision energy. The faster component appears to evolve from having a significant proportion of forward-scattered intensity at 3.26 eV collision energy to predominately backscattered intensity at the higher collision energy. The faster component also appears to increase in relative intensity, with increasing collision energy, compared to the thermal component, which suggests a correlation with the increasing part of the $C_2H_3^+$ cross section (Fig. 1).

For propane reactions at 1.0 eV, TOF data are shown in Fig. 6 for two of the products with larger cross sections, $C_3H_7^+$ and $C_2H_4^+$. In either case, the TOF spectrum is dominated by a thermal component, with a small faster component. The faster component is weaker for the $C_3H_7^+$ channel. For $C_3H_7^+$ at the higher collision energies, the fast tail essentially gives way to the thermal component. The TOF data for $C_2H_3^+$ from propane reactions at the higher collision energies show behavior similar to that seen in the ethane case, a dominant thermal constituent and a persistent faster component, however, the trend towards backscattering of the non-thermal contribution occurs already at 3.67 eV.

The top frame in Fig. 7 shows TOF data for two of the prevalent products deriving from *n*-butane reactions at 1.0 eV collision energy. The $C_3H_7^+$ and $C_3H_5^+$ ions again show the dominant thermal component, with a marginal faster component. At higher energies, the $C_3H_7^+$ behavior parallels that seen for the same product of the propane reactions. As for the two smaller alkanes, the $C_2H_3^+$ product of *n*-butane reactions, at the higher energies, exhibits TOF spectra with a significant fast component, which trends towards backscattering at the highest energy studied.

DISCUSSION

The cross sections presented above support the picture that reactions of O^+ with ethane, propane, and *n*-butane are dominated by a dissociative charge-transfer (DCT) mechanism. In this scenario, interactions involve a quasiresonant electron transfer occurring at primarily large impact parameters, with negligible momentum transfer between colliding

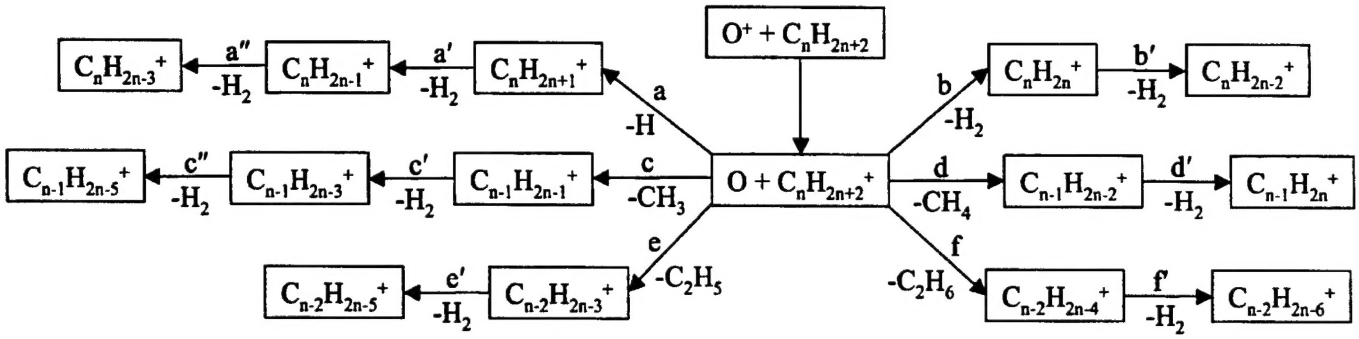

FIG. 8. Dissociative charge-transfer reaction scheme used to account for all but a few minor product ions observed in the $O^+ + C_2H_6/C_3H_8/n\text{-}C_4H_{10}$ reactions. The essential features of the dissociation pathways comprise either an initial simple bond cleavage (left side) or a four-center reaction (right side), with subsequent fragmentations involving loss of H_2. The primed and nonprimed letters denoting the various channels are inserted in the text, in parentheses, where the relevant channels are discussed.

moieties. Since $O(^1D)$ formation is spin forbidden it may be expected that nearly all of the reaction exothermicity, indicated in Eqs. (1)–(3), resides in the nascent alkane ions, thus imparting internal energies to the charge-transfer product ions that are above their respective dissociation limits. The DCT mechanism accounts for the very large total cross sections and the general form of their energy dependences, decreasing with collision energy at near-thermal energies and leveling-off at higher collision energies. The same mechanism has been proposed to explain the results for studies of other ions reacting with ethane, propane, and *n*-butane where charge transfer is also exothermic.[6–9]

Fragmentation pathways for the DCT mechanism are outlined for the present systems in Fig. 8. Such paths have been elucidated in photoionization or electron impact ionization studies of the alkanes, from which fragmentation breakdown curves as a function of ionization energy are derived for ionized ethane, propane, and *n*-butane.[10,25–27] Each of the larger individual cross sections shown in Figs. 1–3 results from a single fragmentation step of the charge-transfer product alkane ion, involving either a simple bond cleavage [loss of $\cdot H$, $\cdot CH_3$, $\cdot C_2H_5$, reactions (a), (c), and (e), in Fig. 8] or a four-center reaction [loss of H_2, CH_4, C_2H_6, reactions (b), (d), and (f), in Fig. 8].[26] The loss of H_2 from ionized ethane, the most efficient channel in the present reaction of ethane and in the electron impact ionization mass spectrum of ethane,[28] has been of particular theoretical[12,25] and experimental[11,29] interest because the transition state indicates migration of an H atom between carbon atoms.

This initial fragmentation step accounts for the production of $C_2H_5^+$ (1a) and $C_2H_4^+$ (1b) from ethane, $C_3H_7^+$ (2a), $C_3H_6^+$ (2b), $C_2H_5^+$ (2c), and $C_2H_4^+$ (2d) from propane, and $C_4H_9^+$ (3a), $C_3H_7^+$ (3c), $C_3H_6^+$ (3d), $C_2H_5^+$ (3e), and $C_2H_4^+$ (3f) from *n*-butane. All of the associated DCT processes are exothermic. In reference to ionization breakdown curves, the threshold or appearance energy of these fragments is less than the recombination energy of the oxygen atom, 13.618 eV.[17] The very minor channel, $C_4H_8^+$ (3b) from *n*-butane, however, does not follow the magnitude and energy dependence of the other one-step fragmentation products.

Further dissociation of these "primary" DCT product ions depends on whether they are produced with sufficient energy to undergo subsequent fragmentation. Such secondary fragmentations are regarded as occurring typically by the four-center reactions that result in loss of H_2 (all "primed" reactions in Fig. 8).[10] Of the above list of primary DCT products, only the $C_3H_6^+$ and $C_3H_7^+$ ions, from both reactions 2 and 3, can have sufficient internal energy following a resonant charge-transfer process to allow this subsequent fragmentation. For $C_3H_7^+$, the resulting "secondary" dissociation yields $C_3H_5^+$, for which the reaction energies are $\Delta E = -0.47$ eV and $\Delta E = -0.99$ eV, in propane (2a) and *n*-butane (3c) DCT reactions, respectively. As seen in Fig. 3, the $C_3H_5^+$ channel is the dominant reaction pathway for reaction 3, and also exhibits a cross section whose energy dependence is similar to those of the single-step DCT products.

By contrast, although the production of $C_3H_5^+$ via DCT in reaction 2 is exothermic, the appearance energy for this ion, derived from photoionization of propane,[28,30] is slightly higher than the O^+ recombination energy. This may be related to the significantly smaller cross section for $C_3H_5^+$ in reaction 2. The yield is significant, nevertheless, and stresses the point that it cannot be assumed *a priori* that dissociative photoionization branching ratios are equivalent to those of corresponding resonant DCT processes.[31] The small but nonnegligible cross section of this two-step product may be related to the fact that the production of $C_3H_5^+$ by DCT in reaction 2 involves an intermediate primary fragmentation step (2a), in which one of the recoiling partners is a hydrogen atom that is necessarily in the ground state due to its high-lying excited states. The $C_3H_7^+$ intermediate fragment ion therefore contains all the remaining available energy, except for the primary fragmentation recoil energy (i.e., $2.0\,\text{eV} - E_{\text{recoil}}$).

Very similar arguments may be used to account for the behavior observed for the $C_3H_6^+ \rightarrow C_3H_4^+ + H_2$ secondary fragmentation for reactions 2 (b) and 3 (d). For DCT, the reaction energies for these channels are $\Delta E = -0.86$ eV and $\Delta E = -1.41$ eV, respectively. These products, however, are much weaker, which could be related to the significantly smaller precursor $C_3H_6^+$ cross sections in comparison with $C_3H_7^+$.

Of the observed products that cannot be ascribed to direct charge transfer, or the exothermic DCT channels discussed above, two general classes may be discerned. The first includes the $C_2H_2^+$ (b′) and $C_2H_3^+$ (a′) products of reac-

tion 1, $C_2H_2^+$ (d′), $C_2H_3^+$ (c′), and $C_3H_3^+$ (a″), from reaction 2, and $C_2H_3^+$ (e′) and $C_3H_3^+$ (c″) from reaction 3. Except possibly for the last of these product channels, these ions belong to the second trend in energy dependence seen among the cross sections, namely the enhanced reactivity with increasing collision energy, which is consistent with an endothermic mechanism. The necessary energy transfer can occur either through low-impact parameter collisions or through a nonadiabatic mechanism in which broadening of the nascent charge-transfer product state distributions occurs as the collision energy is increased.[32] Thermal energy ($\leqslant$0.05 eV) ion–alkane reaction studies have found that the $C_2H_3^+$ ion is the main product in reactions of these alkanes with ions whose recombination energies are at least 15.6 eV,[6,7] whereas $C_2H_3^+$ is undetected for recombination energies not greater than 14.51 eV,[6,8] including O^+.[18] This last point may be reconciled with the present results, in part, by considering that the very small amount of $C_2H_3^+$ we observe at the lowest collision energies may be less than the flowing afterglow detection limit. The nonzero cross sections at the lowest energies of this work suggest that, since the DCT pathway is endothermic, a chemical reaction initiates the formation of $C_2H_3^+$ at these energies. This reaction, producing OH by hydride abstraction and discussed in detail below in conjunction with the recoil velocity analysis, is sufficiently exothermic to produce $C_2H_5^+$ with enough internal energy to dissociate by loss of H_2. We note that $C_2H_5^+$ produced by this mechanism in the earlier flowing afterglow $O^+ + C_2H_6$ study,[18] in which $C_2H_3^+$ is not observed, may be subject to collisional deactivation.

The second general class of product channels, which represent minor pathways that do not fit into the exothermic DCT picture outlined in Fig. 8, include CH_2^+, from reactions 1 and 2, and $C_2H_6^+$, from reactions 2 and 3. The cross sections for CH_2^+ have the same general energy dependence as the endothermic DCT channels, and would require a "geminal," or three-centered, loss of CH_4 and C_2H_6, respectively. By comparison, the production of this ion in ethane and propane reactions, through a reactive mechanism that produces the corresponding alcohol, is exothermic ($\Delta E = -3.05$ eV and $\Delta E = -3.19$ eV, respectively). The negligible CH_2^+ signals at the lowest energies of this work, however, suggests that chemical reaction does not occur, and may be associated with a large barrier. A similar analysis of the $C_2H_6^+$ products is not possible due to their small yields, the accuracy of which are affected by important interferences from the natural deuterium abundance in the prominent $C_2H_5^+$ products.

The TOF data are generally consistent with the interpretation that DCT dominates the reaction of O^+ with ethane, propane, and *n*-butane. In the case of the nondissociative charge-transfer $C_2H_6^+$ product from ethane, the recoil velocity distribution at 1 eV in Fig. 5 involves purely two-body scattering, and therefore relates directly to the details of the collision events. The slow component in this spectrum is consistent with the thermal velocities expected for ions resulting from large impact parameter, long-range charge transfer, with no momentum transfer. The faster portion peaks near V_{CM}, and appears to involve similar amounts in the forward and backward directions, suggesting that these ions derive from a longer-lived complex, the formation of which should follow an LGS (Ref. 24) energy dependence of $E_T^{-0.5}$. The importance of complex-forming collisions would give rise to the initial steep decline in cross section with collision energy.

The peaking near V_{CM} suggests that many of these collisions involve substantial conversion of kinetic to internal energy, with the concomitant small recoil velocities. The arrow in this plot corresponds to the maximum forward velocity of elastically scattered $C_2H_6^+$. Only the tail of the $C_2H_6^+$ velocity distribution extends to this point, confirming that substantial conversion of collision energy to internal energy occurs in the complex-mediated mechanism. Since $C_2H_6^+$ is metastable, with respect to loss of H_2, when excited to energies exceeding 0.39 eV, it is somewhat surprising that ions resulting from substantial transfer of the 1 eV translational energy, in addition to the 2.09 eV exothermicity, should be observed. A possible explanation is that the surviving ethane ions are formed in the spin-forbidden channel, leading to $O(^1D)$ with an excitation energy of 1.97 eV.[33] These arguments are consistent with the fact that the nondissociative charge-transfer cross sections of propane and *n*-butane are significantly smaller, given the substantially higher exothermicities.

The remainder of the TOF spectra pertain to ionic products that derive from interactions resulting in three or even four recoiling moieties, assuming the DCT mechanism. Therefore drawing conclusions based on these data must rely on the assumption that the ions arising from fragmentations do so with negligible recoil velocity in the secondary and tertiary processes. In studies on electron impact ionization of propane, fragment processes for singly charged propane ions were found to exhibit quasithermal kinetic energy releases,[14] so this suggestion may be reasonable. This assumption is not as important in cases where dissociation results in the loss of light neutral fragments (H,H_2), which carry off most of the recoil velocity.

The TOF spectra for $C_2H_4^+$ from reaction 1 (Fig. 5), $C_2H_4^+$ and $C_3H_7^+$ from reaction 2 (Fig. 6), and $C_3H_5^+$ and $C_3H_7^+$ from reaction 3 (Fig. 7), at the various collision energies, are dominated by large thermal components, which would be expected for these exothermic DCT channels where reaction may occur at long range, with no momentum transfer. These TOF spectra indicate very little contribution from the smaller impact parameter collisions, whether complex-mediated or "rebounding," that give rise to faster products (in the laboratory frame). The same behavior, not shown here, was observed for the $C_2H_5^+$ product from each of the three reactions.

The TOF spectra for the $C_2H_3^+$ product, for each of the alkanes, provide some evidence that this ion derives primarily by the endothermic DCT mechanism indicated above. For example, in Fig. 5, the $C_2H_3^+$ TOF spectra for ethane reactions at 3.26 and 12.0 eV clearly indicate a significant fast component, in the laboratory frame. The evolution of the fast component from forward and backward, at 3.26 eV, to purely backward, at 12.0 eV, and the increasing integral cross section, is indicative of an endothermic process where larger impact parameters transfer the necessary translational energy

to internal energy as the collision energy increases. The arrows in the 3.26 eV TOF data of Fig. 5, which encompass the fast $C_2H_3^+$ component, indicate the maximum forward and backward velocities for this ion, with respect to V_{CM}, assuming that the necessary 1.04 eV of the collision energy is converted to internal energy and that dissociation occurs with zero recoil velocity.

The significant $C_2H_3^+$ component at velocities lower than the minimal allowed DCT laboratory velocity suggests that these ions can be attributed to a process initiated by a chemical reaction, the most likely being hydride abstraction to form $OH+C_2H_5^+$. Hydride abstraction adds an additional 4.4 eV to the exothermicity of the corresponding DCT mechanism (e.g., yielding $O+H+C_2H_5^+$) and thus, for each alkane studied here, can produce alkyl ions with sufficient energy to fragment to $C_2H_3^+$. Moreover, this reaction may occur in a stripping mode, in which the H^- is transferred without substantial momentum transfer,[34] resulting in strong backscattering of the product ions, as observed here. In reactions of $C^+ + C_2H_6$ (Ref. 15) and $CD_3^+ + C_2H_6/C_3H_8$ (Ref. 34) systems in which charge transfer is endothermic, hydride abstraction proceeds by just this mechanism. In the latter experiments,[34] the large impact parameters implied by this direct mechanism are born out by very large cross sections (of the order of 40–50 Å^2 at $E_T = 1$ eV) for hydride abstraction, other channels being relatively minor. In the former work,[15] the strong backscattering was accompanied by kinetic energy release in excess of the spectator stripping model.[35] This was ascribed to the "induced repulsive energy release"[36] that derives from the small skew angle[37] characteristic of the potential-energy surface for the heavy–light–heavy mass combination, which governs the energy partitioning in the exit channel. In the present work, hydride abstraction in O^+ + ethane collisions (skew angle=17.5°) is exothermic by 5.6 eV, and even conversion of as much as 60% of this energy to product recoil energy would still allow dissociation of the strongly backscattered $C_2H_5^+$, to give $C_2H_3^+ + H_2$. For the reactions studied here, hydride abstraction could explain both the non-negligible cross section for the $C_2H_3^+$ product at low collision energy, and the strongly backscattered (thermal) component observed in the TOF spectra.

CONCLUSION

Absolute cross sections for reactions of O^+ with ethane, propane, and *n*-butane have been measured as a function of collision energy in the near-thermal to hyperthermal collision energy range. All three systems have very large total cross sections over the entire investigated collision energy range, signifying efficient long-range charge transfer that produces alkane ions with internal energies comparable to the exothermicity. The cross sections, along with time-of-flight measurements for several product ions at a range of collision energies, have been interpreted in the framework of a dissociative charge-transfer mechanism. A large fraction of the observed channels can be summarized by the DCT scheme outlined in Fig. 8.

Very little evidence is found for complex formation and chemical reaction. The nondissociative charge-transfer reaction of ethane shows the strongest evidence for the formation of a complex associated with efficient translational energy transfer. It is suggested that these products, as well as possibly all nondissociative charge-transfer products, are the result of a spin-forbidden charge-transfer reaction producing excited oxygen atoms, $O(^1D)$. The nonzero cross section of the endothermic DCT product, $C_2H_3^+$, at near-thermal collision energies, as well as a minimal momentum transfer component observed in the recoil velocities, suggest that some of these ions are produced in hydride abstraction reactions.

ACKNOWLEDGMENTS

The authors wish to thank Professor D. C. Jacobs for allowing us access to unpublished results, and Dr. A. A. Viggiano for providing the ethane and butane used in this study. This work was supported by AFOSR under task 2303ES02, and was undertaken in support of the Materials Chemistry in the Space Environment MURI.

[1] R. G. Cooks, T. Ast, T. Pradeep, and V. Wysocki, Acc. Chem. Res. **27**, 316 (1994).
[2] S. T. Arnold, A. A. Viggiano, and R. A. Morris, J. Phys. Chem. A **101**, 9351 (1997); **102**, 8881 (1998).
[3] S. Williams, A. J. Midey, S. T. Arnold, R. A. Morris, A. A. Viggiano, Y. Chiu, D. J. Levandier, R. A. Dressler, and M. R. Berman, J. Phys. Chem. A **104**, 10 336 (2000).
[4] G. H. Mount and H. W. Moos, Astrophys. J. Lett. **224**, L35 (1978).
[5] Z. Herman and B. Friedrich, J. Chem. Phys. **102**, 7017 (1995); Z. Herman, K. Birkinshaw, and V. Pacák, Int. J. Mass Spectrom. Ion Processes **135**, 47 (1994); M. Tsuji, K. Matsumura, H. Kouno, T. Funatsu, and Y. Nishimura, Bull. Chem. Soc. Jpn. **67**, 1781 (1994).
[6] C. Praxmarer, A. Hansel, W. Lindinger, and Z. Herman, J. Chem. Phys. **109**(11), 4246 (1998).
[7] M. Tsuji, H. Kuono, K. Matsumura, T. Funatsu, and Y. Nishimura, J. Chem. Phys. **98**, 2011 (1993).
[8] M. Tsuji, K. Matsumura, T. Funatsu, Y. Nishimura, and H. Obase, Int. J. Mass Spectrom. Ion Processes **135**, 165 (1994); M. Tsuji, K. Matsumura, H. Kouno, M. Aizawa, and Y. Nishimura, J. Chem. Phys. **101**, 8687 (1994).
[9] P. Španel and D. Smith, Int. J. Mass Spectrom. Ion Processes **181**, 1 (1998).
[10] R. Stockbauer, J. Chem. Phys. **58**, 3800 (1973).
[11] K.-M. Weitzel and J. Mähnert, Z. Phys. Chem. (Munich) **195**, 181 (1996); F. Güthe and K.-M. Weitzel, Ber. Bunsenges. Phys. Chem. **101**, 484 (1997); J. Mahnert, F. Güthe, and K.-M. Weitzel, *ibid.* **100**, 1899 (1996); S. M. Bråten, T. Helgaker, E. Uggerud, and T. Vulpius, Org. Mass Spectrom. **28**, 1262 (1993).
[12] K.-M. Weitzel, Int. J. Mass Spectrom. Ion Processes **130**, 1 (1994); Y. Kurosaki and T. Takayanagi, Chem. Phys. Lett. **277**, 291 (1997); Y. Osamura, T. Takeuchi, and K. Nishimoto, Bull. Chem. Soc. Jpn. **61**, 3387 (1988).
[13] K.-M. Weitzel, J. Mähnert, and H. Baumgärtel, Ber. Bunsenges. Phys. Chem. **97**, 134 (1993); T. Takeuchi, M. Yamamoto, K. Nishimoto, H. Tanaka, and K. Hirota, Int. J. Mass Spectrom. Ion Phys. **52**, 139 (1983); S. Olivella, A. Solé, D. J. McAdoo, and L. L. Griffin, J. Am. Chem. Soc. **116**, 11 078 (1994); H. U. Poll, V. Grill, S. Matt, N. Abramzon, K. Becker, P. Scheier, and T. D. Märk, Int. J. Mass Spectrom. **177**, 143 (1998); T. Fiegele, V. Grill, S. Matt *et al.*, Vacuum **63**, 561 (2001); S. Olivella, A. Solé, and D. J. McAdoo, J. Am. Chem. Soc. **118**, 9368 (1996); C. Q. Jiao, C. A. DeJoseph, and A. Garscadden, J. Chem. Phys. **114(5)**, 2166 (2001); K. Furuya, K. Ishikawa, A. Matsuo, and T. Ogawa, Chem. Phys. Lett. **313**, 559 (1999); V. Bachler, J. Phys. Chem. **98**, 6089 (1994); H. von Koch, Ark. Fys. **28**, 559 (1964); E. Pettersson and E. Lindholm, *ibid.* **24**, 49 (1962).
[14] T. Fiegele, C. Mair, P. Scheier, K. Becker, and T. D. Märk, Int. J. Mass Spectrom. **207**, 145 (2001).
[15] R. A. Curtis and J. M. Farrar, J. Chem. Phys. **90**, 862 (1989).

[16] M. R. Sievers, Y.-M. Chen, C. L. Haynes, and P. B. Armentrout, Int. J. Mass Spectrom. **195/196**, 149 (2000); P. B. Armentrout and Y.-M. Chen, J. Am. Soc. Mass Spectrom. **10**, 821 (1999); Y.-M. Chen, M. R. Sievers, and P. B. Armentrout, Int. J. Mass Spectrom. **167/168**, 195 (1997); E. L. Reichert, S. S. Yi, and J. C. Weisshaar, Int. J. Mass Spectrom. **195/196**, 55 (2000); J. Marçalo, J. P. Leal, and A. Pires de Matos, *ibid.* **157/158**, 265 (1996).
[17] S. G. Lias, J. E. Bartmess, J. F. Liebman, J. L. Holmes, R. D. Levin, and W. G. Mallard, *Gas-Phase Ion and Neutral Thermochemistry* (ACS/AIP/NBS, New York, 1988).
[18] G. I. Mackay, H. I. Schiff, and D. K. Bohme, Can. J. Chem. **59**, 1771 (1981).
[19] R. A. Dressler, R. H. Salter, and E. Murad, J. Chem. Phys. **99**, 1159 (1993).
[20] X. Li, Y. L. Huang, G. D. Flesch, and C. Y. Ng, J. Chem. Phys. **106**, 1373 (1997).
[21] D. J. Levandier, R. A. Dressler, Y.-H. Chiu, and E. Murad, J. Chem. Phys. **111**, 3954 (1999).
[22] Y. Ikezoe, S. Matsuoka, M. Takebe, and A. Viggiano, *Gas Phase Ion-Molecule Reaction Rate Constants Through 1986* (Mass Spectroscopy Society of Japan, Tokyo, 1987); S. G. Lias, J. R. Eyler, and P. Ausloos, Int. J. Mass Spectrom. Ion Phys. **19**, 219 (1976).
[23] K. M. Ervin and P. B. Armentrout, J. Chem. Phys. **83**, 166 (1985).
[24] G. Gioumousis and D. P. Stevenson, J. Chem. Phys. **29**, 294 (1958).
[25] Z. Prášil and W. Forst, J. Phys. Chem. **71**, 3166 (1967).
[26] M. L. Vestal, in *Fundamental Processes in Radiation Chemistry*, edited by P. Ausloos (Interscience, New York, 1968), p. 59.
[27] J. Sunner and I. Szabo, Int. J. Mass Spectrom. Ion Phys. **25**, 241 (1977).
[28] http://webbook.nist.gov/chemistry/, NIST Chemistry Webbook, 2003.
[29] F. Güthe, M. Malow, K.-M. Weitzel, and H. Baumgärtel, Int. J. Mass Spectrom. Ion Processes **172**, 47 (1998).
[30] J. W. Au, G. Cooper, and C. E. Brion, Chem. Phys. **173**, 241 (1993).
[31] T. Baer and P.-M. Guyon, in *High Resolution Laser Photoionization and Photoelectron Studies*, edited by I. Powis, T. Baer, and C. Y. Ng (John Wiley & Sons, Ltd., New York, 1995), p. 1.
[32] M. R. Spalburg, J. Los, and E. A. Gislason, Chem. Phys. **94**, 327 (1985); R. A. Dressler, D. J. Levandier, S. Williams, and E. Murad, Comments At. Mol. Phys. **34**, 43 (1998); R. A. Dressler, J. A. Gardner, R. H. Salter, and E. Murad, J. Chem. Phys. **96**, 1062 (1992); R. A. Dressler, S. T. Arnold, and E. Murad, *ibid.* **103**, 9989 (1995).
[33] A. A. Radzig and B. M. Smirnov, *Reference Data on Atoms, Molecules, and Ions* (Springer-Verlag, Berlin, 1985).
[34] S. Märk, C. Schellhammer, G. Niedner-Schatteburg, and D. Gerlich, J. Phys. Chem. **99**, 15 587 (1995).
[35] A. Henglein, K. Lacmann, and G. Jacobs, Ber. Bunsenges. Phys. Chem. **69**, 279 (1965); A. Henglein, in *Ion-Molecule Reactions in the Gas Phase*, edited by P. J. Ausloos (American Chemical Society, Washington, DC, 1966), Vol. 58, p. 63.
[36] A. M. G. Ding, L. J. Kirsch, D. S. Perry, J. C. Polanyi, and J. L. Schreiber, Faraday Discuss. Chem. Soc. **55**, 252 (1973).
[37] J. O. Hirschfelder, Int. J. Quantum Chem., Symp. **3**, 17 (1969).